Journal of the Brazilian Society of Mechanical Sciences and Engineering (2021) 43:452
https://doi.org/10.1007/s40430-021-03060-y

TECHNICAL PAPER

Evaluation of shrinkage and weld line strength of thick flat part in injection moulding process

S. M. Nasir[1,2] · Z. Shayfull[1,2] · S. Sharif[3] · Abdellah El-hadj Abdellah[4] · M. Fathullah[1,2] · N. Z. Noriman[2]

Received: 9 May 2020 / Accepted: 2 June 2021 / Published online: 10 September 2021

Abstract

This paper evaluates the shrinkage and strength of weld line using Design of Experiment and Response Surface Methodology in multi-objective optimisation utilising the injection moulding parameters. A simulation process was conducted to determine the recommended setting of injection moulding parameters and the range of the variable parameters. An experimental work was conducted according to the experimental design, where regression models were established to predict the shrinkage and weld line strength. A new set of process parameters setting was found to achieve the optimum shrinkage and weld line strength of the moulded part. The results of shrinkage and weld line strength using an optimal parameter setting after optimisation process were compared with the results obtained using the recommended setting from Autodesk Moldflow Insight software. It was found that the shrinkages in the normal to and parallel to the melt flow directions were reduced by 5.969% and 4.375%, respectively, through the predicted model generated using RSM. On the other hand, the weld line strength improved by 3.758% as compared to the weld line strength obtained from the recommended setting. The shrinkages in both parallel to and normal to the melt flow directions using multi-objective optimisation were reduced by 5.891% and 4.160%, respectively, while the weld line strength was improved by 3.756%, using the combination of the following parameters; 69.93 °C of coolant inlet temperature, 270 °C of melt temperature, 70 MPa of packing pressure and 8 s of cooling time. The predicted errors ranged between 0.2 and 14.5% during the validation experiments. The packing pressure was found to be the most significant parameter affecting the shrinkage in both parallel to and normal to melt flow directions. The coolant inlet temperature on the other hand was the most significant parameter affecting the weld line strength.

Keywords Shrinkage · Weld line strength · Injection moulding · Response surface methodology (RSM) · Multi-objective optimisation

1 Introduction

The demand for the plastic product is very high in the market as a wide variety of shapes can be produced using the injection moulding process. However, a number of defects usually occur during the process, affecting the quality and cost of the products. The undesirable defects such as weld lines, shrinkages and warpage affect the quality of the moulded parts in terms of their mechanical strength, causing poor overall quality [1–5]. Defects such as weld line occur when plastic melt splits and then recombines at a certain location during the injection moulding process [6]. These defects can be minimised using a good combination of parameters setting during the injection moulding process [7–10]. Numerous research works regarding this problem have recently been conducted due to the ever-growing technologies for quality improvement of injection moulded parts [11–14]. In order

✉ S. M. Nasir
nasirsaad@unimap.edu.my

✉ Z. Shayfull
shayfull@unimap.edu.my

1 Green Design and Manufacture Research Group, Center of Excellence Geopolymer and Green Technology (CEGeoGTech), Universiti Malaysia Perlis, 01000 Kangar, Perlis, Malaysia

2 Faculty of Mechanical Engineering Technology, Universiti Malaysia Perlis, Kampus Tetap Pauh Putra, 02600 Arau, Perlis, Malaysia

3 Faculty of Engineering, Universiti Teknologi Malaysia, 81310 UTM Skudai, Johor, Malaysia

4 Laboratory of Mechanics, Physics and Mathematical Modelling (LMP2M), University of Medea, 26000 Medea, Algeria

to increase the mechanical strength at the critical location on the moulded parts, many researchers had used a variety of techniques such as mechanical assistance [15], thermal assistance[16–18] and material additives methods such as adding fillers to the parent material or blending two or more materials [19, 20]. On the other hand, parameter's optimisation methods were widely used as a technique to improve the strength of the moulded part [21, 22].

The process of strengthening the product especially at the location of weld line formation through mechanical assistance had been found in the early 1980s by Tom et al. [23] in his study of VAIM method using polystyrene (PS) as a moulded material. In the VAIM method, the vibrational forces were used to induce flow of the melted polymer during the filling and packing phases of injection moulding process. In recent years, Lu et al. [24] reported using an ultrasonic oscillations technique which was applied to improve the weld line strength of the moulded parts. Ultrasonic signal from the ultrasonic generator was induced to a core side of the mould via the ultrasonic horn. The ultrasonic oscillations were induced into the mould after the filling phase of the injection moulding process was effective to enhance the weld line strength for PS and PS/HDPE blends. In the following year, Lu et al. [25] utilised the same equipment to improve the mechanism of ultrasonic oscillations that increases the molecular diffusion across the weld line formation. These combined methods resulted in an increase in the weld line strength of the moulded parts.

Kikuchi et al. [15] conducted a study on VAIM technique using polystyrene to improve the mechanical behaviour of the moulded part. The result indicated that the improvement of the strength of the moulded part depends on vibration amplitude, frequency, duration and delay time between the injection start and vibration start. The strength was improved as much as 28% compared to the conventional method. Li & Shen [26] also studied the improvement of mechanical properties of the plastic part using VAIM technique and found that the tensile property of the PP part was increased with an increase in vibration pressure amplitude, but the elongation at the break was decreased.

Xie & Ziegmann [20] studied the weld line strength using PP material which was compounded at various weight fractions (10%, 20%, 30%, 35%) of carbon nanofibres (CNFs) and titanium dioxide (TiO_2) nanoparticles through co-screws internal mixing in microinjection moulding process. Results showed that the weld line strength of moulded part was lower than the virgin PP when the CNFs is filled higher than 10%.

Mechanical and thermal assistance in injection moulding processes are successful techniques to improve the strength of moulded parts, as well as the strength at the weld line position, but the shrinkage problem is not considered concurrently during the improvement. The disadvantages of these techniques include their lack of practicality due to the higher setup cost, and the complex mould design requires higher knowledge and skill during the operation. Due to these reasons, these techniques are not widely used in the industry.

In addition, one of the well-known improvement methods was parameter optimisation which involves Design of Experiment (DOE) and artificial intelligence techniques such as Taguchi method, artificial neural networks (ANN), genetic algorithm (GA) and response surface methodology (RSM) where some parameters were attuned to the suitable value in order to obtain an optimum value of shrinkage and weld line strength [1, 27–30]. Some researchers had also combined more than one optimisation methods known as the hybrid optimisation method [31, 32]. The combination of more than one response is becoming more popular among researchers. This technique is called the multi-objective optimisation method [33, 34].

The improvement of weld line strength and shrinkage on the moulded part by optimising the injection moulding parameters is an alternative technique, as well as simpler and easier to implement. There are many optimisation tools that can be used to improve the strength of weld line, as well as shrinkage, in order to optimise the product quality by using single and multiple objectives (responses) method. The improvement of the weld line strength and shrinkage of the moulded parts should be done in parallel, especially for the part which requires the strength for its functionality with precision critical dimensions. It is hard to find studies which consider both elements (shrinkage and weld line strength) as defects. Therefore, this study focuses on improving both shrinkage and weld line strength using a multi-objective optimisation method. This optimisation technique is powered by response surface methodology (RSM) in choosing the best combination and proposing the minimum shrinkage and maximum weld line strength to the parts.

2 Methodology

Autodesk Moldflow Insight (AMI) software was used for simulation to obtain the recommended processing parameters, as well as the range of selected parameters, while Nessei NEX1000 injection moulding machine was employed for the experimental process. The details of mould design were calculated and designed according to the guideline in ISO standard. Design-Expert software was used to generate the list of experiment and analysis of results using RSM technique [35].

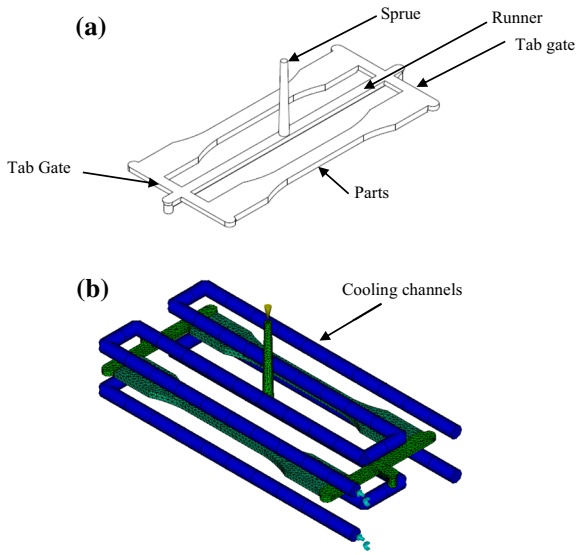

Fig. 1 Thick flat part; **a** feed system design using tab gate; **b** cooling channel design

2.1 Part and mould design

The design of a thick flat part was based on ISO 3167:2002(E) [36] international standard of multipurpose test specimen for plastic injection moulding as shown in Fig. 1a which includes the feed system design. The mould was designed according to part design of ISO 294-1:1996(E) [37] standard for two-cavity mould. The relative runner diameter used in this study is 8 mm. Tab gate was used in this study as recommended in ISO 294-1:1996(E)[37]. The selected material for mould was P20 steel, and the plastic resin was acrylonitrile butadiene styrene (ABS). The properties of ABS are shown in Table 1.

The pressure drop for each design is estimated to determine the significance of the design [35]. The pressure drop, ΔP, is calculated using Eq. 1 [35],

$$\Delta P = \frac{2kL}{R}\left[\frac{\left(3+\frac{1}{n}\right)dotV_{melt}}{\pi R^3}\right]^n \tag{1}$$

where k and n are the reference viscosity ($Pa.s^n$) and power-law index of the polymer melt at the melt temperature, respectively, L is the length of feed system (m), R is the radius of feed system (m) and $\dot{V}_{melt}$ is volumetric flow rate at the inlet (m^3/s). The acceptable pressure drop is below 30 MPa [35].

The cooling time for the runner is estimated to ensure that the runner size does not affect the cooling time of the moulded part. The cooling time for the runner must be less or slightly more than the cooling time for the moulded part

Table 1 Material properties of a plastic resin [30]

Plastic material	ABS
Supplier	Chi Mei Corporation
Trade name/grade	Polylac PA-777B
Material structure	Amorphous
Mould temperature (°C)	40–90
Melt temperature (°C)	220–270
Maximum shear stress (MPa)	0.3
Maximum shear rate (1/s)	50,000
Specific heat, C_p (J/kg°C)	1464.7
Thermal conductivity, k (w/m°C)	0.178
Thermal diffusivity, α (m^2/s)	1.266×10^{-7}
Melt density (g/cm^3)	0.96
Elastic modulus, E (MPa)	2.24×10^3
Poisson's ratio, υ	0.392
Reference viscosity, k ($Pa.s^n$)	17,000
Power law index, n	0.35

[30]. If not, the size of the runner needs to be changed. The cooling time, $t_{c,runner}$, for the runner is calculated using Eq. (2) and the cooling time, $t_{c,\,part}$, for the moulded part is calculated using Eq. (3) [35],

$$t_{c,runner} = \frac{D^2}{23.1(\alpha)} ln\left[0.692\left(\frac{T_{melt}-T_{coolant}}{T_{eject}-T_{coolant}}\right)\right] \tag{2}$$

$$t_{c,part} = \frac{h^2}{\pi^2(\alpha)} ln\left[\left(\frac{4}{\pi}\right)\left(\frac{T_{melt}-T_{coolant}}{T_{eject}-T_{coolant}}\right)\right] \tag{3}$$

where D is the diameter of the runner (m), h is the wall thickness of the moulded part (m), α is the thermal diffusivity of the material (m^2/s), T_{eject} is the specified ejection temperature (°C), $T_{coolant}$ is the coolant temperature (°C) and $T_{melt}$is the melt temperature of the material (°C). The estimated cooling time for the runner can be calculated using Eq. (2) as follows; T_{eject}, $T_{coolant}$, T_{melt} and α are taken from the material properties shown in Table 1.

Apart from the cooling time, shear rate for the gate also needs to be calculated because the gate is the smallest area in the feed system. The shear rate at the gate should not exceed the maximum shear rate allowed as stated for the material properties [35]. The shear rate of this study for dual gate is calculated using Eq. (4) [35],

$$\dot{\gamma} = \frac{2\left(2+\frac{1}{n}\right)\dot{V}}{Wh^2} \tag{4}$$

where n is the power-law index of the polymer melt, $\dot{V}$ is a volumetric flow rate (m^3/s), W is the width of the gate (m) and h is the thickness of the gate (m).

The design of the cooling channel used in this study is illustrated in Fig. 1b according to the requirement proposed in ISO 294-1:1996(E) [37] document. Four channels are needed for each insert to absorb the heat released from the molten plastic as mentioned in ISO 294-1:1996(E) [37]. The size of the cooling channel is estimated by calculating the heat capacity of the moulded part.

The total amount of heat that needs to be removed by the cooling system, $Q_{molding}$ (J) can be calculated using Eq. (5) [35],

$$Q_{molding} = m_{molding}\left(C_p\right)\left(T_{melt} - T_{eject}\right) \tag{5}$$

where $m_{molding}$ is the mass of the moulded part including feed system (kg), C_p is the specific heat of material (J/kg.°C), T_{melt} is the melt temperature (°C) and T_{eject} is the ejection temperature (°C).

With the consideration of the coolant control pressure, ΔP (kPa) and the length of cooling channels, the minimum diameter of the cooling channels can be calculated from Eq. (6) with the allowable pressure drop assumed to be 100 kPa which is half of the maximum pressure supplied from the coolant controller [35]. The coolant pressure drop is due to friction of hoses, turns, plugs and connectors.

$$D_{min} = \sqrt[5]{\frac{\rho_{coolant}\left(L_{line}\right)\left(\dot{V}_{coolant}\right)^2}{\Delta P(10\pi)}} \tag{6}$$

where $\rho_{coolant}$ is density of the coolant (kg/m^3), L_{line} is the total length of the cooling channels at core and cavity sides (m), $\dot{V}_{coolant}$ is the coolant flow rate (m^3/s) and D is the diameter of cooling channels (m).

After the diameter of cooling channel has been estimated, the distance between mould surface and cooling channel is calculated. The linear distance between the cooling channels and the mould surface, H_{line} (m) can be calculated using heat conduction equation state as shown in Eq. (7) [35],

$$h_{conduction} = \frac{K_{mold}}{H_{line}} \tag{7}$$

where $h_{conduction}$ is the convection heat transfer coefficient (W/°C), and K_{mold} is the thermal conductivity of mould material (W/m°C).

By referring to P20 mould steel properties for endurance limit stress and assuming the nominal compressive stress as 150 MPa [35], the value of stress concentration factor, K, in this study is calculated to be 3.51. Thus, in this study, the diameter of the cooling channel was selected to be 8 mm which complies with the calculated values. The distance of cooling channel is selected to be 12 mm as classified within the calculated range.

2.2 Variable parameter and range

Four independent parameters were selected as the variables in this study namely coolant inlet temperature, melt temperature, packing pressure and cooling time based on the previous results of significant parameters that affect shrinkage and weld line strength [21, 38–42]. Coolant inlet temperature was chosen instead of mould temperature because the mould temperature was controlled by coolant inlet temperature.The range of variable parameters was determined based on the recommended simulation results and material specification as shown in Table 2.

2.3 Experimental design and analysis of data

The results obtained from the experiment for shrinkage and strength of weld line were analysed using Design-Expert software with RSM method. All the results from the experiments were arranged in a list of experiments and used to generate a relationship between input parameters setting and output responses which are shrinkage and strength of weld line on the specimen. Two levels of full factorial design were selected using four factors which are coolant inlet temperature (°C), melt temperature (°C), packing pressure (MPa) and cooling time (s). Shrinkages in both parallel to and normal to melt flow directions, and weld line strength were selected as the responses. A list of experiments generated in Design-Expert software based on four factors and four centre points is depicted in Table 3 for Run numbers 1–20. Then, the full factorial design was augmented to RSM using centre composite design (CCD) that consists of additional ten runs as shown in Table 3 for Run numbers 21–30. Based on these results, a model was generated for each response based on the required backward model selection (alpha out = 0.05). The insignificant parameters or interaction between parameters were removed and excluded from the generated models for both shrinkage and strength of weld line. These models were used during the optimisation process.

2.4 Tensile test

Tensile strength, σ_M (N/m^2), was obtained from the maximum tensile stress of the specimen. Universal testing machine (UTM) was used to measure the tensile strength of the moulded part. Extensometer was used as the aid to

Table 2 Selected process variable range for ABS material

Level	Coolant inlet temp. (°C)	Melt temp. (°C)	Packing pressure (MPa)	Cooling time (s)
Minimum	50	250	50	8
Maximum	70	270	70	12

Table 3 List of experiments and results of shrinkage and weld line strength

Experiment type	Run	Variable parameter				Responses		
		Coolant inlet temp. (°C)	Melt temp. (°C)	Packing pressure (MPa)	Cooling time (s)	Shrinkage (%)		Weld line strength (N/mm^2)
						Normal to the melt flow direction	Parallel to the melt flow direction	
Full factorial	1	50	250	70	8	1.33	0.51	40.2451
	2	70	270	70	8	1.06	0.46	41.5181
	3	70	250	70	8	1.07	0.48	41.1915
	4	60	260	60	10	1.55	0.58	40.4282
	5	50	250	50	8	1.67	0.67	40.5520
	6	70	250	70	12	1.30	0.49	40.7418
	7	50	270	50	12	1.68	0.66	40.2625
	8	70	270	50	8	1.53	0.64	40.7765
	9	50	250	70	12	1.24	0.53	40.0301
	10	70	250	50	8	1.66	0.67	40.5995
	11	50	270	70	12	1.09	0.49	40.0180
	12	60	260	60	10	1.60	0.60	40.4561
	13	50	270	50	8	1.65	0.67	40.4126
	14	50	250	50	12	1.68	0.68	40.4964
	15	70	250	50	12	1.69	0.60	40.8620
	16	60	260	60	10	1.58	0.59	40.4531
	17	70	270	70	12	1.14	0.46	41.2646
	18	60	260	60	10	1.58	0.59	40.4520
	19	70	270	50	12	1.66	0.65	40.8541
	20	50	270	70	8	1.37	0.50	40.5764
CCD	21	60	260	60	10	0.62	1.63	40.5862
	22	40	260	60	10	0.65	1.69	40.0241
	23	80	260	60	10	0.56	1.60	41.5126
	24	60	280	60	10	0.56	1.59	40.7475
	25	60	260	60	14	0.60	1.61	40.3665
	26	60	240	60	10	0.61	1.63	40.7867
	27	60	260	60	10	0.59	1.56	40.7257
	28	60	260	60	6	0.58	1.61	40.5623
	29	60	260	80	10	0.31	1.08	41.1588
	30	60	260	40	10	0.72	1.75	40.7076

increase the accuracy of the data collected. The speed of testing used in this study was 50 mm/min according to ISO 527-1:2012 [43]. Five specimens were used for tensile testing for each set of moulding conditions.

2.5 Shrinkage measurement

Shrinkage was measured according to the ISO 294-4:2001 [44] standard to determine the shrinkage of the moulded part. The shrinkage measurement (post-moulding) was measured 48 h after the moulding process.

The specimens were trimmed from the gating system just after the moulding process and stored at room temperature between 16 and 24 h. Five specimens for each of the mouldings were selected for shrinkage measurement. The results of the moulding shrinkage measurement can be calculated for shrinkage in parallel to the melt flow direction, S_{Mp} (%) and normal to the melt flow direction, S_{Mn} (%).

3 Results and discussion

3.1 Analyses of full factorial experiment

The results of average shrinkage and weld line strength for full factorial experiments are shown in Table 3, row numbers 1 until 20. Average shrinkages were calculated based on the shrinkage values both parallel to and normal to the melt

flow direction in both cavities. Besides, weld line strength was obtained from the maximum stress of the thick flat part during the tensile test. The minimum value of shrinkages in both normal to and parallel to the melt flow directions for full factorial experiments is 1.06 mm and 0.46 mm, respectively, and maximum weld line strength is 41.5181 N/mm^2. From these results, Analysis of Variance (ANOVA) was conducted for each response in order to analyse the curvature of the model that will be created. The shrinkages and weld line strength can be improved using response surface methodology (RSM) if the curvature is present in the model.

3.2 Significant factors affecting shrinkage and weld line strength

Table 4 shows the percentage contribution of each factor and significant interaction for shrinkage and weld line strength obtained from ANOVA. The most significant factor of shrinkage for both normal to and parallel to the melt flow directions was packing pressure with 85.24% and 90.64% contribution, respectively. Packing pressure influenced the density of the molten plastic during the packing process. Packing pressure plays a vital role to pack the molten plastic until the solid density is achieved, since the density of polymer varies from melt to solid. Change in packing pressure will also affect the density of molten plastic that leads to the shrinkage issue. Results also showed that coolant inlet temperature, melt temperature and cooling time contributed less significantly towards shrinkage in this study.

Besides, the highest percentage contribution of parameter for weld line strength is the coolant inlet temperature with 59.37%. Therefore, the coolant inlet temperature was the most significant factor that affected the weld line strength of the moulded part. The coolant inlet temperature significantly affects the mould temperature, where the increase in the mould temperature resulted in diffusion on the molecular chains to a higher degree of bonding at the weld line interface. This molecular chain affects the quality of the bonding and the strength of the moulded part. The mould temperature was also found to be the most significant parameter affecting the weld line strength of the moulded part by Annicchiarico & Alcock [45].

Table 4 Percentage contribution of factors

Response	Main factor	
	Factor	Percentage contribution (%)
Shrinkage (normal)	A: Coolant inlet temp	1.70
	B: Melt temp	1.15
	C: Packing pressure	85.24
	D: Cooling time	0.22
Shrinkage (parallel)	A: Coolant inlet temp	3.66
	B: Melt temp	0.62
	C: Packing pressure	90.64
	D: Cooling time	0.01
Weld line strength	A: Coolant inlet temp	59.37
	B: Melt temp	2.03
	C: Packing pressure	1.29
	D: Cooling time	3.93

3.3 Analysis results of shrinkage in normal to the melt flow direction

Table 5 shows a statistical analysis of ANOVA for two-level factorial of shrinkage in both normal to and parallel to the material flow directions, and weld line strength. ANOVA results indicated several significant terms to the response, including main factors and interactions. The probability values less than 0.05 (p value < 0.05) were considered to have a significant effect [46]. Meanwhile, insignificant terms (p value > 0.05) have been removed in order to obtain an accurate empirical model based on the backward elimination regression with alpha out to exit being 0.05. The significant terms model was determined with 95% of confidence level that was applied in an ANOVA analysis. From the analysis, the probability values (p value) below 0.05 indicate that analysis of shrinkage in normal to and parallel to the material flow model is significant with p value < 0.0001 [46]. Meanwhile, the curvature is significant because the p value is less than 0.05. Thus, it is possible that a quadratic model is a better fit compared to a linear model [46]. Therefore, the models are best fit with second-order models rather than first-order by augmenting axial runs to allow quadratic terms to be incorporated into the model. Data were augmented using rotatable central composite design (CCD) to produce a quadratic model. The CCD is a very efficient design for fitting the second-order model or response surface [47]. It requires additional 10 axial runs with two replication of centre runs as recommended by the Design-Expert software.

The models of shrinkage in the normal to and parallel to the melt flow directions, as well as weld line strength, are developed based on the CCD results. These models are used to predict the best combination of parameters in order to

Table 5 Summary of ANOVA results for shrinkage in normal and parallel directions to the melt flow, and weld line strength

Source	Shrinkage (Normal)	Shrinkage (Parallel)	Weld line strength
Model	Significant (p value < 0.0001)	Significant (p value < 0.0001)	Significant (p value < 0.0001)
Curvature	Significant (p value $= 0.0012$)	Significant (p value $= 0.0128$)	Significant (p value $= 0.0032$)

reduce shrinkages, as well as increase the weld line strength of the moulded part. The results for all responses are shown in Table 3 starting from run 21–30.

3.4 Analysis results of CCD for shrinkage in normal to the melt flow direction

The ANOVA of shrinkage in normal to melt flow direction after augmentation of full factorial experimental design is shown in Table 6. The results showed that the model is significant with several model terms. The block gives the lowest sum of square value compared to other terms which indicated that the variation between block 1 and 2 is not critical. As shown in Table 6, the interaction of AC and the main effects of A, B and C are significant to the model. After fitting the first-order model, the result shows that only packing pressure (C) gives a quadratic effect to the model. Besides, the lack of fit (LOF) value is 0.0932 (p value > 0.05) which satisfies the model to be fitted.

The values of R^2 and Adjusted R^2 are very high which are close to 1 (≈0.9377 and ≈0.9243) indicating that the model is desirable. The Adjusted R^2 has a difference of only 0.0681 with Predicted R^2 which implies that it is in reasonable agreement (< 0.2). On the other hand, the value of adequate prediction is above 4 (≈ 28.9702), which indicates that the model is adequate [46].

Furthermore, the main effects plot namely coolant inlet temperature (A), melt temperature (B) and packing pressure (C), on the shrinkage in normal to the melt flow direction, are shown in Fig. 2a–c, respectively. The plot of shrinkage versus coolant inlet temperature shows that an increase in temperature reduces the shrinkage. This result is in line with the documented research works where the shrinkage on the moulded parts was reduced with an increase in mould temperature due to better pressure transmission [48]. The same pattern is shown for melt temperature, while an increase in the melt temperature resulted in a decrease in shrinkage in normal to the melt flow direction [49]. These mould and melt temperatures affected the stress relaxation of the moulded material. High mould and melt temperature will cause the material to be more 'relaxed' during the cooling process [50]. Cooling rate has a significant effect on the degree of relaxation [50]. Thus, rising the mould and melt temperature will reduce the shrinkage by allowing the material to 'relax'. Meanwhile, the shrinkage in the normal to the melt flow direction decreased with the increase in packing pressure which is in agreement with other research works [49, 51, 52]. Increasing the packing pressure resulted in the increase in the density of polymer melt. The shrinkage was reduced when the melt density increased as close as solid density of the moulded material. Therefore, shrinkage was reduced when the packing pressure increased.

Figure 2d shows the contour plot of interaction between coolant inlet temperature (A) and packing pressure (C). The response line of both factors tends to crossover, indicating that the interaction is significant. It can be seen that by increasing the coolant inlet temperature with packing pressure at high level (70 MPa), the shrinkage in normal to the melt flow direction was decreased drastically. On the other hand, at the lowest packing pressure setting (50 MPa),

Table 6 ANOVA of CCD for shrinkage in normal direction to the melt flow

Source	Sum of squares	df	Mean square	F value	p value Prob > F	Summary
Block	0.0721	1	0.0721			
Model	1.1266	5	0.2253	69.2310	< 0.0001	Significant
A-coolant inlet temp	0.0330	1	0.0330	10.1410	0.0041	
B-melt temp	0.0176	1	0.0176	5.4091	0.0292	
C-packing pressure	0.9560	1	0.9560	293.7447	< 0.0001	
AC	0.0189	1	0.0189	5.8092	0.0243	
C^2	0.1011	1	0.1011	31.0510	< 0.0001	
Residual	0.0749	23	0.0033			
Lack of fit	0.0711	19	0.0037	4.0200	0.0932	Not significant
Pure error	0.0037	4	0.0009			
Cor total	1.2735	29				
Additional information						
Standard deviation	0.0570					
Mean	1.5057					
R^2	0.9377					
Adj R^2	0.9242					
Pred R^2	0.8561					
Adequate precision	28.9702					

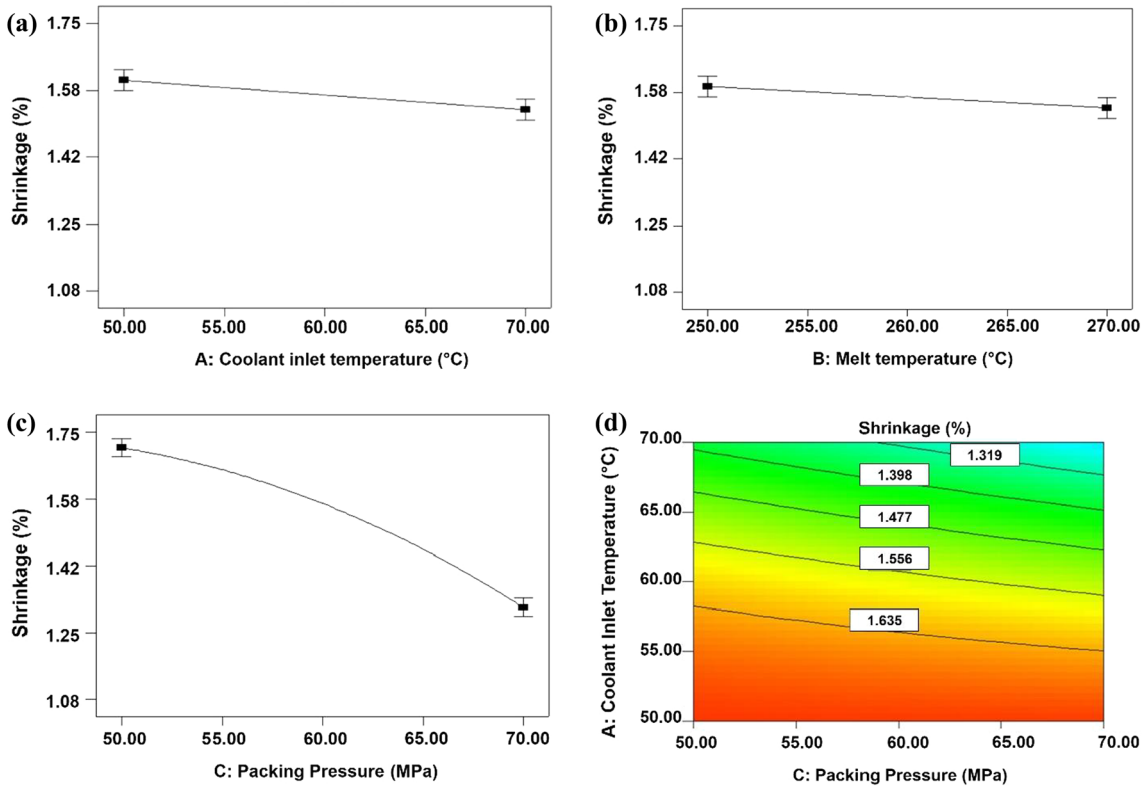

Fig. 2 Main effect plot for factor, **a** coolant inlet temperature, **b** melt temperature, **c** packing pressure, **d** contour plot of interaction coolant inlet temperature and packing pressure to the shrinkage

increasing the coolant inlet temperature from 50 to 70 °C showed no significant effect on the shrinkage. The contour plots can be used to estimate the effect of the interaction between variables and responses [45]. The contour graph in Fig. 2d reveals that the lowest shrinkage can be achieved when packing pressure is set at a high level (70 MPa) and the coolant inlet temperature is at a high level (70 °C). This finding is in agreement with Altan [49].

The empirical model generated by the Design-Expert software was used to estimate the response of shrinkage in normal to the melt flow direction at a different setting within the range investigated. The empirical models in terms of actual factor are shown in Eq. (8),

$$\begin{aligned}\left(Shrinkage_{normal}\right) = {} & 0.32456 + 0.016917A - 2.70832 \times 10^{-3}B \\ & + 0.07175C - 3.4375 \times 10^{-4}AC - 5.92361 \times 10^{-4}C^2\end{aligned} \tag{8}$$

where A is the coolant inlet temperature (°C), B is the melt temperature (°C) and C is the packing pressure (MPa).

The experimental and predicted results of shrinkage in the normal to the melt flow direction are illustrated in Fig. 3. Overall, the experimental results are in line with the results from the empirical model. Therefore, the empirical model has a good prediction in predicting the shrinkage values with 9.06% error between average experimental results and predicted results.

3.5 Analysis results of CCD for shrinkage in parallel to the melt flow direction

Table 7 shows an ANOVA result of shrinkage in parallel to the melt flow direction after augmentation of full factorial experimental design. The sum of square value for the block is 0.00004 which shows that the variations between blocks are not critical (≈ 0). Besides, the model is significant with p value lower than 0.0001. Coolant inlet temperature (A), melt temperature (B) and packing pressure (C) are significant parameters where the of "Prob > F" is less than 0.05 [45]. No interaction between parameters has been found as significant for shrinkage in parallel to the melt flow direction. Moreover, the lack of fit (LOF) is not significantly (p value > 0.05) relative to the pure error which satisfies the model to be fitted.

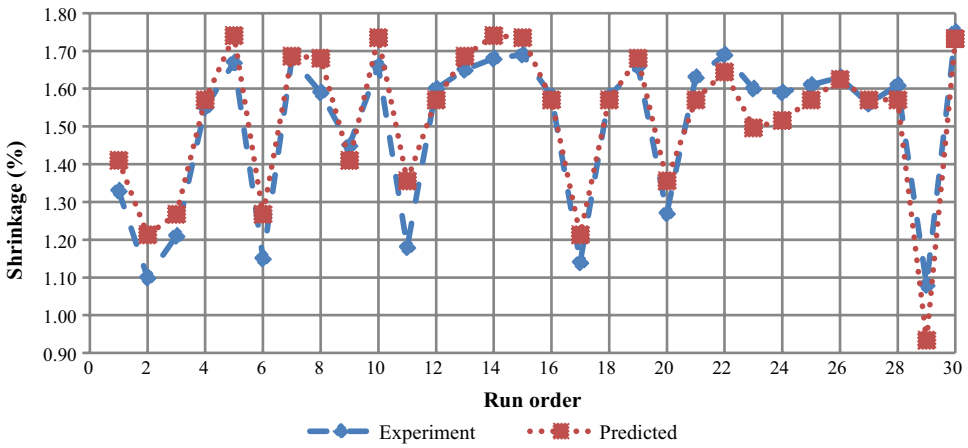

Fig. 3 Experimental and predicted results of shrinkage in normal direction to the melt flow using CCD

Table 7 ANOVA of CCD for shrinkage parallel to melt flow direction

Source	Sum of squares	df	Mean square	F value	*p* value Prob > F	Summary
Block	0.00004	1	0.0000			
Model	0.20721	4	0.0518	157.5374	< 0.0001	Significant
A-coolant inlet temp	0.00756	1	0.0076	22.9951	< 0.0001	
B-melt temp	0.00144	1	0.0014	4.3837	0.0470	
C-packing pressure	0.18809	1	0.1881	572.0011	< 0.0001	
C^2	0.01012	1	0.0101	30.7696	< 0.0001	
Residual	0.00789	24	0.0003			
Lack of fit	0.00720	20	0.0004	2.0797	0.2505	Not significant
Pure error	0.00069	4	0.0002			
Cor total	0.21515	29				
Additional information						
Standard deviation	0.0181					
Mean	0.5771					
R^2	0.9633					
Adj R^2	0.9572					
Pred R^2	0.9105					
Adequate precision	43.6654					

The R^2 and Adjusted R^2 have high values which are close to 1 (≈0.9633 and ≈0.9572), hence, are desirable. There is only 0.0467 difference between Adjusted R^2 and Predicted R^2 which is in a reasonable agreement because the value is below 0.2 [45]. The adequate prediction is above the value of 4 (≈ 436,654), indicating that the model is adequate.

The main effect plot for coolant inlet temperature (A), melt temperature (B) and packing pressure (C) is shown in Fig. 4a–c, respectively. Shrinkage versus coolant inlet temperature plot (Fig. 4a) illustrated that the shrinkage is minimum with the increase in the coolant inlet temperature. This result shows a similar pattern with shrinkage in normal to the melt flow direction and agreed with previous researchers where the shrinkage on the moulded parts was reduced when the mould temperature was increased [42]. The trend for the shrinkage in both (parallel and normal) to the melt flow directions is in line with the finding from previous researcher [42]. Besides, packing pressure showed a quadratic relation towards shrinkage, and the graph shows that the shrinkage was decreased with the increase in packing pressure [49, 51, 52]. The contour plots obtained in this study were used to estimate the effect of the interaction to the response when the parameters are at high and low levels [45]. No interaction was found for the shrinkage parallel to the melt flow direction. The results from the contour plot (Fig. 4d) showed that shrinkage was reduced with the increase in packing pressure, as well as coolant inlet temperature. This finding agreed with that of Chen [53] in the study of reducing shrinkage of the moulded part.

The empirical model for the shrinkage parallel to the melt flow direction in terms of actual factors is expressed in Eq. (9),

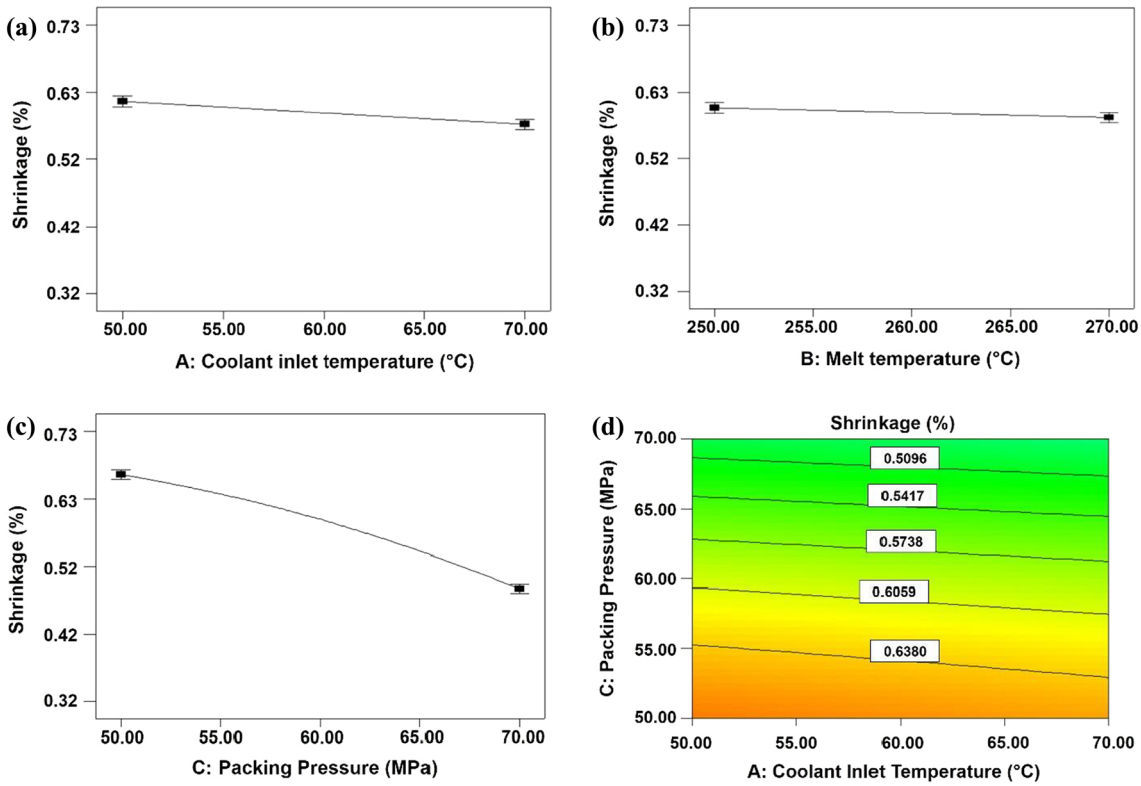

Fig. 4 Main effect plot for, **a** coolant inlet temperature, **b** melt temperature, **c** packing pressure and **d** contour plots of coolant inlet temperature and packing pressure

$$\left(Shrinkage_{parallel}\right) = 0.75694 - 1.775 \times 10^{-3}A - 7.5 \times 10^{-4}B + 0.013639\mathrm{C} - 1.87435 \times 10^{-4}C^{2} \quad (9)$$

where A is coolant inlet temperature (°C), B is melt temperature (°C) and C is packing pressure (MPa).

The experimental and predicted results of shrinkage parallel to the melt flow direction are illustrated in Fig. 5. The generated graph of experimental versus shrinkage parallel to the melt flow direction has yielded a good prediction, whereas the pattern shows similarity between the experimental results and empirical model. Error of average value between experiment and predicted model is 1.72%, indicating that the model has a very good relation with the experimental results.

3.6 Analysis of results of CCD for weld line strength

The analysis of results from CCD for weld line strength of the moulded part implies that the model is significant (p value < 0.05) as shown in Table 8. This means that there is less than 0.0001% chance for F-Value of model occurring

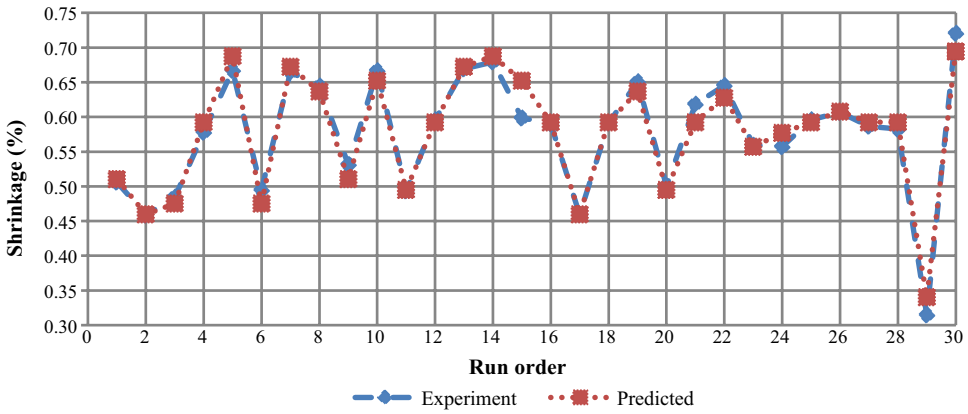

Fig. 5 Experimental and predicted results of shrinkage in parallel to the melt flow using CCD

Table 8 ANOVA of CCD for weld line strength

Source	Sum of squares	df	Mean square	F value	*p* value Prob > F	Summary
Block	0.0782	1	0.0782			
Model	4.1400	11	0.3764	31.8144	< 0.0001	Significant
A-coolant inlet temp	2.7962	1	2.7962	236.3665	< 0.0001	
B-melt temp	0.0327	1	0.0327	2.7662	0.1146	
C-packing pressure	0.1165	1	0.1165	9.8509	0.0060	
D-cooling time	0.1253	1	0.1253	10.5908	0.0047	
AB	0.0719	1	0.0719	6.0809	0.0246	
AC	0.3838	1	0.3838	32.4402	< 0.0001	
BC	0.1178	1	0.1178	9.9578	0.0058	
CD	0.1622	1	0.1622	13.7078	0.0018	
A^2	0.0783	1	0.0783	6.6145	0.0198	
B^2	0.0773	1	0.0773	6.5335	0.0205	
C^2	0.2477	1	0.2477	20.9422	0.0003	
Residual	0.2011	17	0.0118			
Lack of fit	0.1909	13	0.0147	5.7457	0.0522	Not significant
Pure error	0.0102	4	0.0026			
Cor total	4.4193	29				
Additional information						
Standard deviation	0.1088					
Mean	40.6456					
R^2	0.9537					
Adj R^2	0.9237					
Pred R^2	0.8167					
Adequate precision	22.1196					

due to noise [45]. Coolant inlet temperature (A), packing pressure (C) and cooling time (D) have significant impacts, while AB, AC, BC and CD indicated significant interactions in the model (p value < 0.05). The terms A^2, B^2 and C^2 are also significant (p value < 0.05) in establishing the polynomial model. The lack of fit (LOF) is insignificant (p value > 0.05) which indicates that the quadratic model is fitted.

From Table 8, the R^2 (0.9537) value is acceptable for the model (≈ 1). The predicted R^2 is in reasonable agreement with the adjusted R^2 where the difference between them is below 0.2, which is only 0.107 in this study. The adequate precision value is above 4 (≈22.1196) which shows that the model is adequate.

Figure 6a–d shows the main effect of weld line strength of the moulded part for terms A, B, C and D, respectively. Terms A, B and C illustrated that the curvature is significant (p value < 0.05) representing the second-order terms in the model. Coolant inlet temperature (A) indicates a positive effect on the weld line strength of the moulded part, where an increase in coolant inlet temperature resulted in an increase in the weld line strength due to the fact that the molecular chains gained higher ability to flow at a higher temperature [45]. On the other hand, with the lower temperature of coolant inlet, the molecular diffusion and subsequent molecular bonding in weld interface are incomplete, so, it weakens the interaction of the molecular chain. Thus, the strength of the weld line area is weak. This result is in line with that of Chen et al. [54] in their study on thin wall part.

The same trend is illustrated for term B (melt temperature) as shown in Fig. 6b, but the line is slightly decreased near the middle and tends to increase subsequently. This term contributes to the increase in the melt temperature resulting in increasing the weld line strength. The molecules carry higher energy at higher melt temperature. This energy decreases when the melt material enters the mould cavities due to lower mould temperature compared to the barrel. Thus, higher melt temperature carries more molecular energy bonding compared to low melt temperature. This result is in line with those of Chen et al. [54] and Ozcelik et al. [41].

The trend of factor C (packing pressure) also illustrated similar trend with A and B as shown in Fig. 6c. Increasing the packing pressure led to an increase in the weld line strength. Low pressure at the flow front of material does not promote molecular chain entanglement, resulting in poor strength of the moulded part. This result agrees with a research by Chen et al. [54] and Ozcelik et al. [41].

In this study, cooling time (D) was found as a significant factor for weld line strength of the moulded part. The

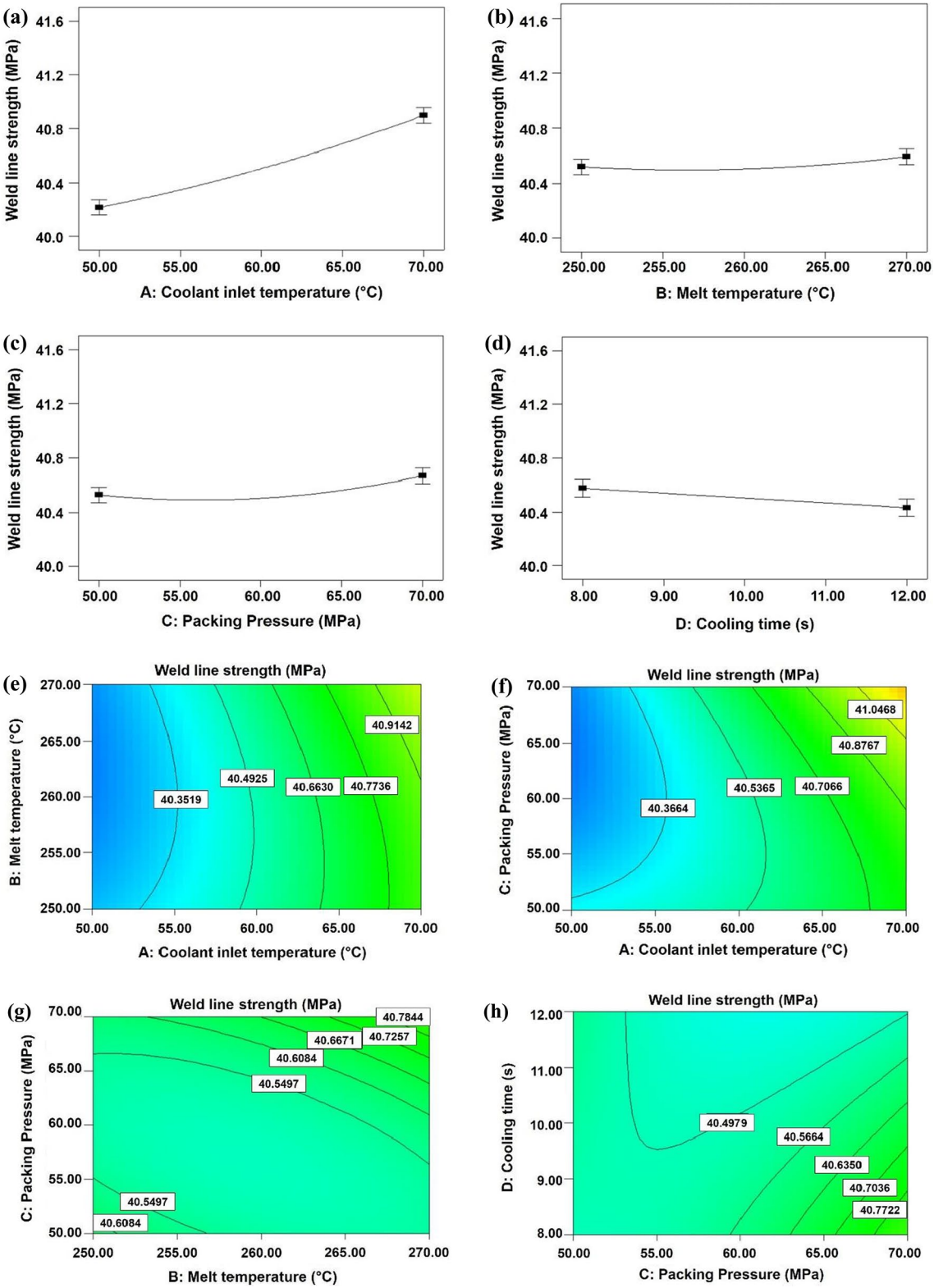

Fig. 6 Main effect of weld line strength on the moulded part for terms for, **a** coolant inlet temperature, **b** melt temperature, **c** packing pressure and **d** cooling time, contour plots of **e** melt temperature and coolant inlet temperature, **f** packing pressure and coolant inlet temperature, **g** packing pressure and melt temperature and **h** cooling time and packing pressure

graph shown in Fig. 6d indicates that weld line strength decreases with an increase in cooling time. Residual stress on the moulded parts depends on the cooling rate where the cooling rate after the moulded part was ejected from the mould is faster than the cooling stages inside the mould [55]. Thus, shorter cooling time in the mould increases the residual stress of the part. Furthermore, tensile stress on the moulded part is increased with the increase in residual stress [56].

Figure 6e illustrates the contour plots of factors A and B at packing pressure of 50 MPa and cooling time of 10 s. The maximum strength of the moulded part is achieved at high melt temperature (270 °C) and high coolant inlet temperature (70 °C). The contour plot of factors A (coolant inlet temperature) and C (packing pressure) at melt temperature of 260 °C and cooling time of 10 s are shown in Fig. 6f. High packing pressure (70 MPa) and high coolant inlet temperature (70 °C) increase the weld line strength. The contour plots of factors B (melt temperature) and C (packing pressure) at coolant inlet temperature of 60 °C and cooling time of 10 s are shown in Fig. 6g, respectively. The interaction of BC (B is melt temperature; C is packing pressure) showed similar trends with the interaction of AB (A is coolant inlet temperature; B is melt temperature) and AC (A is coolant inlet temperature; C is packing pressure) where the maximum weld line strength can be achieved at high packing pressure (70 MPa) and high coolant inlet temperature (70 °C). Figure 6h illustrates the contour plots of factors C (packing pressure) and D (cooling time) at coolant inlet temperature of 60 °C and melt temperature of 260 °C. Differing from other interactions, the interaction of CD shows that the weld line strength is optimal when the cooling time is at the minimum parameter (8 s) with the maximum packing pressure (70 MPa).

The empirical model of the weld line strength in terms of the actual factors is shown in Eq. (10),

$$\begin{aligned} Strength_{WL} = {} & 104.64646 - 0.29657A - 0.36123B - 0.36159C + 0.2659D \\ & + 6.70528 \times 10^{-4}AB + 1.54873 \times 10^{-3}AC + 8.58055 \times 10^{-4}BC \\ & - 50337 \times 10^{-3}BC + 5.28646 \times 10^{-4}A^2 + 5.25396 \times 10^{-4}B^2 \\ & + 9.40648 \times 10^{-4}C^2 \end{aligned} \tag{10}$$

where A is coolant inlet temperature (°C), B is melt temperature (°C), C is packing pressure (MPa) and D is cooling time (s).

The experimental and predicted results of weld line strength are illustrated in Fig. 7. The generated graph of experimental versus predicted results of weld line strength showed a similar pattern. It can be concluded that the predicted value is in a very good agreement with the experimental results because the error between experiment and predicted values is about 0.20%. Based on the predicted model of CCD, the result of optimisation of shrinkages and weld line strength is discussed in the next section.

3.7 Optimisation result of CCD

The predicted optimal solution of parameters for the shrinkage in both parallel to and normal to the melt flow directions, and the weld line strength of the moulded part using RSM are concluded in Table 9. To obtain the significant result of this study, the optimal solution of the parameters in experimental works was compared to the recommended value

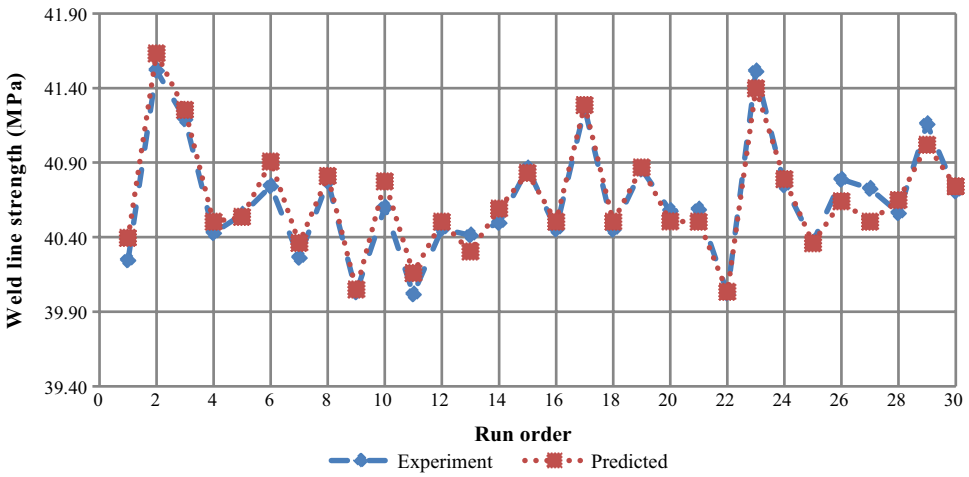

Fig. 7 Experimental and predicted results of the weld line strength using CCD

Table 9 Predictive optimal solution of shrinkage and the weld line strength in multi- and separate objectives

Variable/response	Item	Recommended setting	Multi-objectives	Separate objectives			Improvement (%)	
							Separate objectives	Multi-objectives
Variable	Coolant inlet temp. (°C)	53	69.93	70	70	69.99		
	Melt temp. (°C)	270	270	270	270	269.87		
	Packing pressure (MPa)	70	70	70	70	70		
	Cooling time (s)	12	8	8.11	8.56	8		
Response	Shrinkage (normal) (%)	1.29	1.214	1.213	N/A	N/A	5.969	5.891
	Shrinkage (parallel) (%)	0.48	0.460	N/A	0.459	N/A	4.375	4.160
	Weld line strength (MPa)	40.12	41.627	N/A	N/A	41.628	3.758	3.756

obtained from the simulation. Results showed that shrinkage was reduced significantly by 5.969% and 4.375% in normal to and parallel to the melt flow direction, respectively, while the weld line was improved 3.758% compared to the recommended setting from the simulation. Meanwhile, the reduction in shrinkage in parallel to and normal to the melt flow direction using multi-objective optimisation was 5.891% and 4.160%, respectively, and the weld line strength of the moulded part was increased by 3.759%. These improvements are according to the combination of parameters setting used during experimental works to improve the shrinkage and weld line strength on the moulded part.

The result of shrinkages and weld line strength in multi-objectives is found to be almost similar. Therefore, the multi-objective optimisation using RSM was preferable due to the same parameters that were employed to obtain the minimum shrinkage, as well as the maximum weld line strength conditions.

3.8 Verification test

A series of verification tests were conducted in order to validate the predicted model solutions. Three empirical models had been generated using ANOVA in Design-Expert software, by comparing the results from prediction and confirmation tests using the following equation;

$$Error = \left| \frac{Result\ of\ conformation\ tests - Predicted\ value}{Result\ of\ conformation\ tests} \right| \times 100 \tag{11}$$

The verification results from all experiments are represented in Table 10. The results indicated that the predicted errors ranged from 0.2 to 14.5%. The prediction system is in good agreement with the verification experiments where the errors are below 20% [57].

Table 10 Results of verification test

	Responses	Variable				Predicted value (RSM)	Actual value	Error (%)
		Coolant inlet temp. (°C)	Melt temp. (°C)	Packing pressure (MPa)	Cooling time (s)			
Separate objective	Shrinkage (normal)	70	270	70	8.11	1.214%	1.08%	12.3
	Shrinkage (parallel)	70	270	69.99	11.79	0.460%	0.45%	2.2
	Weld line strength	69.99	269.87	70	8	41.627 MPa	41.52 MPa	0.3
Multi-objectives	Shrinkage (normal)	69.93	270	70	8	1.213%	1.06%	14.5
	Shrinkage (parallel)					0.459%	0.46%	0.2
	Weld line strength					41.628 MPa	41.52 MPa	0.3

4 Conclusions

Optimisation process using RSM has been applied to find the best parameters setting in order to reduce shrinkage and increase the weld line strength, through injection moulding process. Packing pressure was found to be the most significant factor affecting the shrinkage, while the coolant inlet temperature had the most significant effect on the weld line strength. Final result revealed that the coolant inlet temperature of 69.93 °C, melt temperature of 270 °C, packing pressure of 70 MPa and cooling time of 8 s are the best combination of parameters to reduce the shrinkage up to 5.969% and increase the weld line strength up to 3.758% compared to the values from the recommended setting obtained from the simulation in experimental research. Validation process shows that the prediction system is in good agreement with the verification experiments with an error of less than 14.5%.

Acknowledgements We would like to acknowledge the reviewer(s) for the helpful advice and comments provided. The authors wish to thank the Ministry of Education, Malaysia, for their financial support of this study through Fundamental Research Grant Scheme (FRGS), FRGS/1/2019/TK03/UNIMAP/02/20.

References

1. Oliaei E, Heidari BS, Davachi SM, Bahrami M, Davoodi S, Hejazi I, Seyfi J (2016) Warpage and shrinkage optimization of injection-molded plastic spoon parts for biodegradable polymers using Taguchi, ANOVA and artificial neural network methods. J Mater Sci Technol 32(8):710–720
2. Fischer JM (2013) Handbook of molded part shrinkage and warpage, 2nd edition. Plastics design library. William Andrew, Inc, USA
3. Harper CA (2006) Handbook of plastic processes. Wiley
4. Osswald T, Hernández-Ortiz JP (2006) Polymer processing—modeling and simulation. Hanser Publishers
5. Lee M, Kwon YS, Lee CK (2019) Effect of warpage on the operation of a rapid cooling and heating device. J Braz Soc Mech Sci 41(8):322
6. Kim KH, Park JC, Suh YS, Koo BH (2017) Interactive robust optimal design of plastic injection products with minimum weldlines. Int J Adv Manuf Tech 88(5–8):1333–1344
7. Kashyap S, Datta D (2015) Process parameter optimization of plastic injection molding: a review. Int J Plast Technol 19(1):1–18
8. Sánchez-Sánchez X, Elias-Zuñiga A, Hernández-Avila M (2018) Processing of ultra-high molecular weight polyethylene/graphite composites by ultrasonic injection moulding: taguchi optimization. Ultrason Sonochem 44:350–358
9. Kitayama S, Miyakawa H, Takano M, Aiba S (2017) Multi-objective optimization of injection molding process parameters for short cycle time and warpage reduction using conformal cooling channel. Int J Adv Manuf Tech 88(5–8):1735–1744
10. Hentati F, Hadriche I, Masmoudi N, Bradai C (2019) Optimization of the injection molding process for the PC/ABS parts by integrating Taguchi approach and CAE simulation. Int J Adv Manuf Tech 104(9–12):4353–4363
11. Chen WC, Nguyen MH, Chiu WH, Chen TN, Tai PH (2016) Optimization of the plastic injection molding process using the Taguchi method, RSM, and hybrid GA-PSO. Int J Adv Manuf Technol 83(9):1873–1886
12. Xu G, Yang ZT, Long GD (2012) Multi-objective optimization of MIMO plastic injection molding process conditions based on particle swarm optimization. Int J Adv Manuf Tech 58(5–8):521–531
13. Kitayama S, Onuki R, Yamazaki K (2014) Warpage reduction with variable pressure profile in plastic injection molding via sequential approximate optimization. Int J Adv Manuf Techno 72(5–8):827–838
14. Erzurumlu T, Oktem H (2007) Comparison of response surface model with neural network in determining the surface quality of moulded parts. Mater Des 28:459–465
15. Kikuchi A, Coulter JP, Gomatam RR (2006) Assessing the effect of processing variables on the mechanical response of polysytrene molded using vibration-assisted injection molding process. J Appl Polym Sci 99:2603–2613
16. Wang G, Zhao G, Guan Y (2012) Thermal response of an electric heating rapid heat cycle molding mold and its effect on surface appearance and tensile strength of the molded part. J Appl Polym Sci 128(3):1339–1352
17. Zhao G, Wang G, Guan Y, Li H (2011) Research and application of a new rapid heat cycle molding with electric heating and coolant cooling to improve the surface quality of large LCD TV panels. Polym Adv Technol 22:476–487
18. Saifullah ABM, Masood SH, Sbarski I (2012) Thermal–structural analysis of bi-metallic conformal cooling for injection moulds. Int J Adv Manuf Technol 62(1–4):123–133
19. Lu C, Guo S, Wen L, Wang J (2004) Weld line morphology and strength of polystyrene/polyamide-6/poly (styrene-co-maleic anhydride) blends. Eur Polym J 40:2565–2572
20. Xie L, Ziegmann G (2011) Mechanical properties of the weld line defect in micro injection molding for various nano filled polypropylene composites. J Alloys Compd 509:226–233
21. Ozcelik B (2011) Optimization of injection parameters for mechanical properties of specimens with weld line of polypropylene using Taguchi method. Int Commun Heat Mass 38(8):1067–1072
22. Dorf T, Ferrer I, Ciurana J (2019) The effect of weld line on tensile strength of polyphenylsulfone (PPSU) in ultrasonic micromoulding technology. Int J Adv Manuf Tech 103(5–8):2391–2400
23. Tom AM, Kikuchi A, Coulter JP (2008) Experimental determination of optimized vibration-assisted injection molding processing parameters for atactic polystyrene, specialized molding techniques: application, design, materials and processing. Cambridge University Press
24. Lu C, Yu X, Guo S (2005) Ultrasonic improvement of weld line strength of injection-molded polystyrene and polystyrene/polyethylene blend parts. Polym Eng Sci 45:1666–1672
25. Lu C, Yu X, Guo S (2006) The mechanism of ultrasonic improvement of weld line strength of injection molded polystyrene and polystyrene/polyethylene blend parts. J Polym Sci 44:1520–1530
26. Li Y, Shen K (2008) Improving the mechanical properties of polypropylene via melt vibration. J Appl Polym Sci 109(1):90–96
27. Heidari BS, Oliaei E, Shayesteh H, Davachi SM, Hejazi I, Seyfi J, Bahrami M, Rashedi H (2017) Simulation of mechanical behavior and optimization of simulated injection molding process for PLA based antibacterial composite and nanocomposite bone screws using central composite design. J Mech Behav Biomed Mater 65:160–176
28. Chen WC, Kurniawan D, Fu GL (2012) Optimization of process parameters using DOE, RSM, and GA in plastic injection molding. Adv Mat Res 472–475:1220–1223

29. Kurtaran H, Erzurumlu T (2005) Efficient warpage optimization of thin shell plastic parts using response surface methodology and genetic algorithm. Int J Adv Manuf Technol 27:468–472
30. Heidari BS, Moghaddam AH, Davachi SM, Khamani S, Alihosseini A (2019) Optimization of process parameters in plastic injection molding for minimizing the volumetric shrinkage and warpage using radial basis function (RBF) coupled with the k-fold cross validation technique. J Polym Eng 39(5):481–492
31. Chen WJ, Lin JR (2012) Design of optimization parameters with hybrid genetic algorithm method in multi-cavity injection molding process. Adv Mat Res 463–464:587–591
32. Yin F, Mao H, Hua L (2011) A hybrid of back propagation neural network and genetic algorithm for optimization of injection molding process parameters. Mater Des 32:3457–3464
33. Wang G, Zhao G, Li H, Guan Y (2011) Multi-objective optimization design of the heating/cooling channels of the steam-heating rapid thermal response mold using particle swarm optimization. Int J Therm Sci 50:790–802
34. Li K, Yan S, Zhong Y, Pan W, Zhao G (2019) Multi-objective optimization of the fiber-reinforced composite injection molding process using Taguchi method, RSM, and NSGA-II. Simul Model Pract Theory 91:69–82
35. Kazmer DO (2007) Injection mold design engineering. Hanser Publishers
36. ISO 3167 (2002) Plastics—Multipurpose test specimens
37. ISO 294–1 (1996) Plastics—Injection moulding of test specimens of thermoplastic materials — Part 1: General principles, and moulding of multipurpose and bar test specimens
38. Kitayama S, Natsume S (2014) Multi-objective optimization of volume shrinkage and clamping force for plastic injection molding via sequential approximate optimization. Simul Model Pract Th 48:35–44
39. Chen CP, Chuang MT, Hsiao YH, Yang YK, Tsai CH (2009) Simulation and experimental study in determining injection molding process parameters for thin-shell plastic parts via design of experiments analysis. Expert Syst Appl 36:10752–10759
40. Chiang KT, Chang FP (2006) Application of grey-fuzzy logic on the optimal process design of an injection-molded part with a thin shell feature. Int Commun Heat Mass 33:94–101
41. Ozcelik B, Kuram E, Topal MM (2012) Investigation the effects of obstacle geometries and injection molding parameters on weld line strength using experimental and finite element methods in plastic injection molding. Int Commun Heat Mass 39:275–281
42. Chen CC, Su PL, Lin YC (2009) Analysis and modeling of effective parameters for dimension shrinkage variation of injection molded part with thin shell feature using response surface methodology. Int J Adv Manuf Technot 45:1087–1095
43. ISO 527–1 (2012) Plastics—determination of tensile properties—Part 1: general principles
44. ISO 294–4 (2001) Plastics—Injection moulding of test specimens of thermoplastic materials—Part 4: determination of moulding shrinkage
45. Annicchiarico D, Alcock JR (2014) Review of factors that affect shrinkage of molded part in injection molding. Mater Manuf Process 29(6):662–682
46. Montgomery DC (2009) Design and analysis of experiments, 7th edn. Wiley
47. Chang TC, Faison E III (1999) Optimization of weld line quality in injection molding using an experimental design approach. J Inj Molding Technol 3(2):61
48. Jou YT, Lin WT, Lee WC, Yeh TM (2014) Integrating the Taguchi method and response surface methodology for process parameter optimization of the injection molding. Appl Math Inform Sci 8:1277–1285
49. Altan M (2010) Reducing shrinkage in injection moldings via the Taguchi, ANOVA and neural network methods. Mater Des 31:599–604
50. Shoemaker J (2006) Moldflow design guide. Hanser Publishers, Munich
51. Alam MM, Kumar D (2013) Reducing shrinkage in plastic injection moulding using Taguchi method in Tata magic head light. Int J Sci Res 2(2):107–110
52. Chen CC, Su PL, Chiou CB, Chiang KT (2011) Experimental investigation of designed parameters on dimension shrinkage of injection molded thin-wall part by integrated response surface methodology and genetic algorithm: A case study. Mater Manuf Process 26:534–540
53. Chen CS, Chen SC, Liao WH, Chien RD, Lin SH (2010) Micro injection molding of a micro-fluidic platform. Int Commun Heat Mass 37(9):1290–1294
54. Chen CS, Chen TJ, Chien RD, Chen SC (2007) Investigation on the weldline strength of thin-wall injection molded ABS parts. Int Commun Heat Mass 34:448–455
55. Guevara-Morales A, Figueroa-López U (2014) Residual stresses in injection molded products. J Mater Sci 49:4399–4415
56. Kamal MR, Lai-Fook RA, Hernandez-Aguilar JR (2002) Residual thermal stresses in injection moldings of thermoplastics: a theoretical and experimental study. PolymEng Sci 42(5):1098–1114
57. Desai KM, Survase SA, Saudagar PS, Lele SS, Singhal RS (2008) Comparison of artificial neural network (ANN) and response surface methodology (RSM) in fermentation media optimization: case study of fermentative production of scleroglucan. Biochem Eng J 41:266–273